Phys Chem Minerals (2002) 29: 112–121
DOI 10.1007/s00269-001-0226-2
© Springer-Verlag 2002

ORIGINAL PAPER

W. Lottermoser · K. Steiner · M. Grodzicki
K. Jiang · G. Scharfetter · J. W. Bats · G. Redhammer
W. Treutmann · S. Hosoya · G. Amthauer

The electric field gradient in synthetic fayalite α-Fe_2SiO_4 at moderate temperatures

Received: 8 August 2001 / Accepted: 27 September 2001

Abstract This work reports on the evaluation of the electric field gradient (efg) in synthetic fayalite α-Fe_2SiO_4 using three different procedures: (1) experimental, with single-crystal Mössbauer spectroscopy (SCMBS) on the three principal sections of an α-Fe_2SiO_4 sample for several temperatures in the range 20 °C ≤ T ≤ 300 °C; (2) semiquantitative, with the on-line calculation of the efg from three-dimensional difference electron densities, and (3) a fully quantitative method with cluster molecular orbital calculations based on the density functional theory. The experimental efg is in good agreement with our previously published low-temperature data as well as with the results obtained by the fully quantitative approach. In the latter case, large cluster sizes (up to 97 atoms) are necessary to obtain quantitative agreement with experiment. This is also considered as being responsible for the lack of correspondence with the semiquantitative efg on M1. Previously reported symmetry violations on the M2 site are also confirmed by our SCMBS measurements.

W. Lottermoser (✉) · K. Steiner · M. Grodzicki
G. Redhammer · G. Amthauer
Institute of Mineralogy, Hellbrunnerstrasse 34III,
A-5020 Salzburg, Austria
e-mail: werner.lottermoser@sbg..ac.at
Fax: + 43 662 8044 622

K. Jiang
Department of Physics, East China Normal University,
Shanghai 200062, China

G. Scharfetter
Department of Computer Sciences, Jakob-Haringer-Strasse 4,
5020 Salzburg, Austria

J. W. Bats
Institute of Organic Chemistry, University of Frankfurt,
Marie-Curie-Strasse 11, 60439 Frankfurt am Main, Germany

W. Treutmann
Institute of Mineralogy, Petrology and Crystallography,
Hans-Meerwein-Strasse, 35032 Marburg, Germany

S. Hosoya
Institute of Inorganic Synthesis, Yamanashi University,
Kofu 400, Japan

Keywords Electric field gradient · Synthetic fayalite

Introduction

The electric field gradient (efg) tensor is a central quantity when studying the relationship between structural and chemical properties in solids, because it provides a most sensitive measure for the symmetry and intensity of the electric charge distribution around a given nucleus on a certain crystallographic site.

Generally, the efg tensor is the second derivative of the electrostatic potential $\partial^2 V/\partial x_i \partial x_j$ and geometrically represented by a tensor ellipsoid with the semiaxes V_{xx}, V_{yy}, V_{zz} with the conventional order $|V_{zz}| \geq |V_{yy}| \geq |V_{xx}|$. Especially in the case of low site symmetries, the evaluation of this tensor concerning its direction and magnitude is non-trivial, but strongly revealing for certain physical properties. Experimentally, there are two main methods to obtain an efg: nuclear quadrupole resonance (NQR) and Mössbauer spectroscopy – the latter is applied in the present study. Two parameters which can be refined in a Mössbauer pattern in favourable cases, the quadrupole splitting QS and the asymmetry parameter η, representing the flattening of the efg ellipsoid, yield the direction and size of the efg. Additionally, from single-crystal spectra the orientation of the efg tensor with respect to the crystallographic axes can be derived from the intensity distribution of the Mössbauer peaks with two angle parameters β and α (see, e.g. Gonser 1975).

Theoretically, we use two approaches: (1) a so-called semiquantitative approach calculating the field gradient from experimental three-dimensional deformation (difference electron) densities derived from X-ray diffraction refinements and (2) a so-called fully quantitative calculation of the efg tensor by an electronic structure method based on density functional theory. The first method is based on the assumption that aspherical electron densities, as produced by Fourier inversions of the difference between observed total structure factors and the

calculated spherical ones, may represent in our case *d*-electron distributions around a given nucleus and therefore provide the main contribution to the efg. The second (fully quantitative approach) is commonly regarded as the state-of-the-art treatment of compounds with moderately complicated structures, i.e. with about 100 atoms per unit cell, and should also shed light on the limits of the semiquantitative approach, as mentioned, e.g. in an investigation on aluminum phosphate (Thong and Schwarzenbach 1979, and references therein).

The object of our investigation is synthetic fayalite α-Fe_2SiO_4 which has been chosen for several reasons:

- An experimental efg is well established for the low-temperature region by Mössbauer spectroscopy (Lottermoser et al. 1996); a comparison with our present study at moderate temperatures (between room temperature and 300 °C) should be easily achieved.
- With regard to the semiquantitative and fully quantitative method the crystallographic structure is also well established (Fuess et al. 1981; Fujino et al. 1981). The latter authors have already published deformation density maps that should represent *d*-electron distributions because of the chosen procedure (Fujino et al. 1981). These can be directly compared to the 3-D deformation density maps forming the basis of our semi-quantitative evaluation of the efg. The fully quantitative treatment is based on the accurate positional parameters and lattice parameters.
- The structure is complex enough to supply interesting results such as the canted arrangement of magnetic moments on the M1 position at low temperatures, but not too complicated to become unfeasible with the semiquantitative and fully quantitative methods. The probably different efgs on the two non-equivalent sites M1 ($\bar{1}$symmetry) and M2 (symmetry *m*) will provide insight into the problem of why the magnetic properties behave so differently for the two sites.

Accordingly, the aim of our investigation is first to compare our three approaches with each other using a sample with a high probability of good results and, second, to answer the question to what extent the point charge model, applied at the semiquantitative level, can supply rather easy-to-obtain results comparable with the most sophisticated procedures such as the fully quantitative method.

Experimental and evaluation of the spectra

The experimental conditions and the provenance of our fayalite single crystal are identical to those described in our previous work (Lottermoser et al. 1995, 1996) with one exception. The three sections with the crystallographic axes *a*, *b*, *c* parallel to the **k** vector of the incident γ-rays, respectively, had to be carefully embedded in a special epoxy glue in order to prevent oxidation during heating, which was performed in a self-constructed furnace for each section between room temperature and 300 °C with a step width of 50 °C.

The corresponding Mössbauer spectra were fitted with our recently developed refinement routine based on a genetic algorithm (Lottermoser et al. 1999; Steiner et al. 1999) and, for verification of the validity of the parameters, with a conventional fit program (Lottermoser et al. 1988). In particular, the well-resolved patterns at 300 °C could easily be decomposed into two subspectra which can be associated with each of the two crystallographic sites (subspectrum A ≡ M1, B ≡ M2). The corresponding parameters are displayed in Table 1 and have the usual meaning:
Isomer shift δ relative to α-iron (mm s)^1 at room temperature
Half width Γ of the lines with Lorentzian shape (mm/s)
Quadrupole splitting $QS = \frac{1}{2}eQV_{zz}\,(1 + \eta^2/3)^{1/2}$ (mm/s)
... with $V_{zz} = \mathrm{efg} = z$ component of the efg tensor and $Q =$ nuclear quadrupole moment
Asymmetry parameter $\eta = (V_{xx} - V_{yy})/V_{zz}$
Angle β between the **k** vector of the incident γ-rays (≡ **a** or **b** or **c**, respectively) and V_{zz} [°]

Angle α between the projection of **k** in the (V_{xx}, V_{yy})-plane and V_{xx} [°]

The χ^2 value of the final fit was taken as a criterion for the quality of the refinement:

$$\chi^2 = \sum_1^N (Y_{i,\mathrm{cal}} - Y_{i,\mathrm{obs}})^2 / Y_{i,\mathrm{obs}}^2 \; 1/(N-K) \;\; ,$$

where $Y_{i,\mathrm{cal}}$ and $Y_{i,\mathrm{obs}}$ are calculated and observed intensities per channel *i*, respectively, *N* is the total channel number and *K* the number of refined parameters.

From the experimental angle values the corresponding orientational angles of the efg axes were calculated with respect to the crystallographic axes and are displayed in Table 2.

As an example for all three sets of Mössbauer spectra, the patterns of the measurement with **k**//**a** are displayed in Fig. 1 for the different temperature settings from room temperature to 300 °C – the other sets differ in the intensity distribution for the two subspectra; this difference determines the different orientational angles β and α defined above.

The refinement itself was performed following the premises of our previous studies (Lottermoser et al. 1995, 1996). However, as can be seen by inspection of the spectra of Fig. 1, the system is severely overdetermined by the comparably high amount of refined parameters. Thus, we had to introduce some (soft) constraints in order to obtain reliable results:

- For a given temperature, the Mössbauer parameters of one kind should be identical within error bars for all three sections (with the exception of the angle parameters).
- As the measured sections are cut from the same specimen, the area distribution should be identical (within the error bars) for all three samples.
- The evaluated efg should not differ considerably from that of our low-temperature results (cf. Lottermoser et al. 1996), as structural phase transitions have not been observed in the considered temperature range.
- The axes of the efg tensor should form a 90° tripod (with a certain tolerance of about 10° for reasons of slight misorientations of the different sections), as already discussed in our previous study (Lottermoser et al. 1996).

Semiquantitative method

The basic principles of the procedure presented in this section are so well established (e.g. Buerger 1977) that only a brief overview on the formalism is given here. Its true three-dimensional verification, however, is something quite new and will be referred to in more detail.

With the derivation of structure factors from intensity distributions (X-ray or neutron diffractometry) we formally obtain a Fourier synthesis of the electronic distribution $\rho(x, y, z)$ in the considered unit cell:

Table 1 Mössbauer parameters of fayalite single crystal sections with **k**//**a**, **b**, **c**, respectively, at different temperatures. Isomer shift δ relative to α-iron, half width Γ, quadrupole splitting QS asymmetry parameter η, orientational angles β and α and goodness-of-fit parameter χ^2. **Errors are given in** *round brackets*; where the error exceeds the parameter value, an *x* is marked instead

T (°C)	δ (mm/s)	Γ (mm/s)	QS (mm/s)	η	β (°)	α (°)	χ^2
k//**a**							
RT							
A	1.130 (9)	0.30 (3)	2.72 (3)	0.65	122.9 (9)	329 (3)	0.48
B	1.156 (7)	0.33	2.94 (2)	0.86	89.96	−181	
100							
A	1.07 (1)	0.28 (3)	2.53 (4)	0.65	125 (1)	335 (4)	0.41
B	1.120 (9)	0.31	2.85 (3)	0.86	79 (2)	−206 (2)	
150							
A	1.03 (1)	0.27 (2)	2.41 (5)	0.65	122 (1)	325 (4)	0.43
B	1.09 (1)	0.29	2.78 (3)	0.86	90.0 (x)	−181	
200							
A	0.98 (2)	0.27 (7)	2.24 (7)	0.65	120 (2)	322 (5)	0.43
B	1.04 (2)	0.296 (2)	2.67 (5)	0.86	89.96 (x)	−181	
250							
A	0.95 (2)	0.266 (2)	2.15 (7)	0.65	119 (2)	317 (5)	0.41
B	1.01 (2)	0.292	2.60 (5)	0.86	89.96 (x)	−181	
300							
A	0.93 (2)	0.26 (4)	2.04 (7)	0.8 (5)	120 (2)	321 (5)	0.44
B	0.99 (1)	0.286	2.52 (4)	0.79 (7)	86 (15)	−192 (5)	
k//**b**							
RT							
A	1.13 (1)	0.30 (3)	2.75 (3)	0.65	54.2 (9)	233 (3)	0.48
B	1.17 (1)	0.296	2.95 (5)	0.86	−27.2 (7)	78 (11)	
100							
A	1.07 (1)	0.28 (3)	2.54 (3)	0.65	55.5 (8)	240 (3)	0.48
B	1.13 (1)	0.284	2.84 (5)	0.86	−26.7 (7)	90	
150							
A	1.04 (1)	0.28 (3)	2.42 (3)	0.65	56.4 (8)	243 (4)	0.46
B	1.10 (1)	0.280	2.78 (5)	0.86	−25.8 (7)	90	
200							
A	1.00 (1)	0.27 (2)	2.26 (3)	0.56 (9)	58.0 (8)	253 (6)	0.44
B	1.06 (1)	0.280	2.67 (5)	0.93 (8)	−23.7 (7)	90	
250							
A	0.97 (1)	0.26 (4)	2.16 (5)	0.65	57 (1)	263	0.44
B	1.03 (2)	0.278	2.61 (8)	0.86	−23 (1)	90	
300							
A	0.93 (2)	0.26 (3)	2.05 (6)	0.7 (2)	59 (2)	278 (18)	0.40
B	1.00 (2)	0.280 (2)	2.5 (1)	0.9 (2)	−23 (2)	90	
k//**c**							
RT							
A	1.1 (1)	0.2 (2)	2.8 (7)	0.65	21 (12)	1.9	0.39
B	1.17 (6)	0.236 (4)	2.9 (1)	0.86	90	90	
100							
A	1.07 (4)	0.22 (8)	2.5 (2)	0.65	28 (4)	−392 (31)	0.43
B	1.12 (2)	0.242 (2)	2.82 (6)	0.86	74 (3)	90	
150							
A	1.0 (1)	0.2 (3)	2.4 (9)	0.65	24 (13)	1.9	0.39
B	1.09 (7)	0.224 (4)	2.7 (2)	0.86	84 (28)	90	
200							
A	0.99 (8)	0.2 (2)	2.2 (5)	0.65	30 (8)	1.9	0.41
B	1.04 (4)	0.240 (2)	2.65 (9)	0.86	102 (8)	90	
250							
A	0.96 (9)	0.2 (2)	2.1 (6)	0.65	34 (9)	1.9	0.36
B	1.02 (5)	0.234 (2)	2.6 (1)	0.86	78 (9)	108 (12)	

$$F(\mathbf{h}) = \int \rho(x,y,z) e^{2\pi i \mathbf{h}\mathbf{r}} \mathrm{d}V \ ,$$

with the structure factor F, $\mathbf{h}$ = reciprocal lattice vector and x, y, z = fractional coordinates within the cell.

Vice versa, it is possible to obtain ρ as the Fourier inversion from experimental (observed) or calculated structure factors

$$\rho(\mathbf{r}) = \int F(\mathbf{h}) e^{-2\pi i \mathbf{h}\mathbf{r}} \mathrm{d}V^*$$

In practice, we have to evaluate a triple sum over the discrete h, k, ls

$$\rho(x,y,z) = \sum_h \sum_k \sum_l A_{hkl} e^{-2\pi i(hx+ky+lz)} \ ,$$

Table 2 Angles of the efg components on M1 and M2 (synth. fayalite) with respect to the crystallographic axes in deg. (SG Pnma) according to the three applied methods: *Exp* means experimental: *Semi* semiquantitative; *Full* full-quantitative approach

	M1			M2		
	V_{xx}	V_{yy}	V_{zz}	V_{xx}	V_{yy}	V_{zz}
Exp						
a	48.4	123.8	120.0	178.9	89.0	89.9
b	63.5	39.5	117.0	90.0	113.0	23.0
c	55.5	88.9	34.5	90.0	−16.5	73.5
Semi						
a	76.9	28.9	64.7	131.4	138.6	90.4
b	158.8	71.2	99.5	89.9	90.6	0.6
c	106.4	111.2	27.3	138.6	48.6	89.5
Full						
a	61.7	130.8	126.2	166.7	76.7	90.0
b	51.2	43.8	107.1	90.0	90.0	0.0
c	51.9	103.3	41.2	76.7	13.3	90.0

with the structure amplitude $|A_{hkl}| = |F_{hkl}| / V_z$, and V_z = volume of unit cell. Provided that the number of structure factors is sufficiently high to avoid series termination errors (Fourier ghosts), it is possible to generate an electron density map of the unit cell of the sample under consideration, very often with surprising details. Additionally, with electron densities from theoretical structure factors and subsequently subtracting them from the observed ones, deformation or difference electron densities are obtained that should yield in our case aspherical density distributions, e.g. from the *d* electrons responsible for the electronic contribution of the efg. A very sophisticated example for these deformation densities is given in the study of Fujino et al. (1981).

Most of these plots, however, have in common that they represent only two-dimensional or at best quasi-three-dimensional sections through the unit cell (as in Fujino's work), resembling the well-known iso-altitude curves in geography.

As the deformation density $\Delta\rho(x, y, z)$ is, in fact, four-dimensional, we tried to establish a method which allows the resulting aspherical electron densities to be displayed as hyperareas in space. For this purpose, we modified a commercial program [IDL$^{(R)}$, Research Systems Inc., developed, e.g. for applications in computer tomography] in such a way that these hyperareas are displayed dependent on their Cartesian coordinates (on the computer monitor or printer) "floating" in space where the fourth coordinate ρ or $\Delta\rho$, respectively, is represented by the transparency of the chosen colour (opacity). These perspective-generating plots were made possible with self-programmed routines, one (EVOX, Steiner et al. 1998) transforming the crystallographic axis system to the obligatory Cartesian basis system (voxel), another accelerating the processing power by a fast Fourier transform (FFT).

Whereas this program system was created for a better display of electron densities, other routines serve for an on-line calculation of the efg: for this purpose, the aspherical densities in question can be highlighted on the computer screen and selected for the calculation (rendering) – the chosen hyperareas are integrated over their volume in space and the resulting efg is then evaluated with respect to a special central ion (in this case Fe^{2+} on M1 and M2, respectively) using the point charge formalism (cf. e.g. Rager and Schmidt 1981). Usually, the charge distribution around the given ion is not axial, so that a diagonalization of the full efg tensor is automatically performed. The resulting eigenvectors and eigenvalues are determined and a graphic representation of the corresponding diagonalized tensor is displayed on the screen in the former deformation density plot. For the M1 and M2 position in synthetic fayalite displayed in Fig. 2, the relevant angles with respect to the crystallographic axes, as calculated from the eigenvectors, and absolute values of the quadrupole splitting and asymmetry parameter, are presented in Table 2.

The crystallographic data underlying the evaluations mentioned above were collected on a Siemens Smart CCD diffractometer using three different spherical single-crystal specimen of synthetic fayalite. Standard reflections remained stable, equivalent ones were averaged. The intensities were corrected for deviations from ideal spherical shape and for lambda-half contributions using program SADABS (Sheldrick 2000). In addition, a spherical absorption correction was made for each crystal. The structure was refined for each of the three datasets using program SHELXL-97 (Sheldrick 1997). Representing the other samples, only the data of sphere no. 1 are displayed in Table 3 – the meaning of the parameters should in most cases be self-explanatory.

Fully quantitative method

Theoretical basis

All calculations were performed in local spin density approximation (LSDA) by the spin-polarized self-consistent charge (SCC) $X\alpha$ method (Grodzicki 1980 and 1985). However, the $X\alpha$ potential (with $\alpha = 0.7$) is used only for the evaluation of the two- and three-centre integrals while the one-centre integrals are derived from all-electron relativistic atomic calculations. Furthermore, the core electrons enter the two- and three-centre integrals via a pseudopotential also derived from relativistic atomic calculations. The method is hence ab initio in the sense that it does not contain any adjustable parameter. The valence basis set consists of 2*s*, 2*p* orbitals for O and F, 3*s*, 3*p* orbitals for Mg and Si, and 3*d*, 4*s*, 4*p* orbitals for Fe.

Within the framework of the LSDA, ionization and excitation energies are usually calculated by the transition state procedure (Slater 1974). In most cases, this leads to a uniform shift of all orbital energies so that energy differences are affected only to a minor extent. Accordingly, *d*–*d* transition energies are determined as the respective orbital energy differences. The calculation of hyperfine parameters within the framework of a valence-electron-only MO method has been described in detail previously (Grodzicki et al. 1987). In particular, the evaluation of the efg tensor $V_{\alpha\beta}$ is based on dividing the charge density into the positive point charges Q_μ^{core} of the ionic cores and the charge distribution arising from the valence electrons:

$$V_{\alpha\beta} = \sum_{\mu\neq 0} Q_\mu^{\text{core}} V_{\alpha\beta}(R_{\mu 0}) - e_0 \sum_{\mu\nu ij} P_{ij}^{\mu\nu} \int \varphi_i^\mu (r - R_{\mu 0}) V_{\alpha\beta}(r) \varphi_j^\nu (r - R_{\nu 0}) d^3 r \ .$$

The iron atom is located at R_0, $R_{\mu 0} = R_\mu - R_0$, e_0 is the (positive) elementary charge, $\varphi_i^\mu(r)$ is the *i*-th atomic orbital at the μth atom, $P_{ij}^{\mu\nu}$ the bond-order matrix, and the tensor operator components $V_{\alpha\beta}(r)$ are given as

$$V_{\alpha\beta}(r) = \frac{1-\gamma(r)}{r^3} \ \frac{3 r_\alpha r_\beta - r^2 \delta_{\alpha\beta}}{r^2} \ ,$$

where the Sternheimer shielding function $\gamma(r)$ arises from the polarization of the core electrons of the iron atom by charges outside the core and has been derived from atomic self-consistent first-order perturbation calculations (Lauer et al. 1979). With respect to a basis set of atomic orbitals, the efg tensor can be decomposed into three different contributions according to the location of the atomic orbitals in the matrix elements:

1. Valence contribution with both atomic orbitals at the iron site, i.e.

$$V_{\alpha\beta}^{\text{val}} = -e_0 \sum_{ij} P_{ij}^{\infty} \int \varphi_i^0(r) V_{\alpha\beta}(r) \varphi_j^0(r) d^3 r \ .$$

The radial part of the remaining one-center integral is proportional to $\langle r^{-3} \rangle (1 - R)$, where the Sternheimer antishielding constant R has the value 0.075 (Lauer et al. 1979) and the expectation value $\langle r^{-3} \rangle$

is derived from relativistic atomic calculations as a function of the valence shell occupation numbers.

2. Covalence contribution with one atomic orbital at the iron site and the other at a ligand atom, i.e.

$$V_{\alpha\beta}^{\mathrm{cov}} = -e_0 \sum_{vij} P_{ij}^{0v} \int \varphi_i^0(r) V_{\alpha\beta}(r) \varphi_j^v(r - R_{v0}) d^3r \ ,$$

that describes the anisotropy of the electronic charge distribution in the iron-ligand bonds.

3. Ligand contribution with both atomic orbitals at ligand atoms, i.e.

$$V_{\alpha\beta}^{\mathrm{lig}} = \sum_{\mu \neq 0} Q_\mu^{\mathrm{core}} V_{\alpha\beta}(R_{\mu 0}) - e_0 \sum_{\mu v ij} P_{ij}^{\mu v} \int \varphi_i^\mu(r - R_{\mu 0}) V_{\alpha\beta}(r) \varphi_j^v(r - R_{v0}) d^3r \ ,$$

where the sum in the electronic part runs over all ligands, i.e. $\mu, v \neq 0$. In this case, the Sternheimer shielding function $\gamma(r)$ can be replaced with γ_∞ having a value of -8.70 (Lauer et al. 1979). It should be emphasized that this definition is not identical with the common use of this term in crystal-field or point-charge approximations. The evaluation of all integrals has been described in detail previously (Grodzicki et al. 1987).

The measured quadrupole splitting ΔE_Q is related to the components of the efg tensor in its principal axes system by

$$\Delta E_Q = 1/2 e_0 Q V_{zz} (1 + \eta^2/3)^{1/2} \ ,$$

where the asymmetry parameter $\eta = (V_{xx} - V_{yy})/V_{zz}$ can take values between 0 and 1 and describes the deviation of the efg from axial symmetry. The size of the nuclear quadrupole moment Q of the first excited state of ^{57}Fe is assumed to be 0.15 barn (Ray and Das 1977; Lauer et al. 1979). In the principal axes system of the efg tensor, the efg V_{zz} is simply the sum of the valence, covalence and

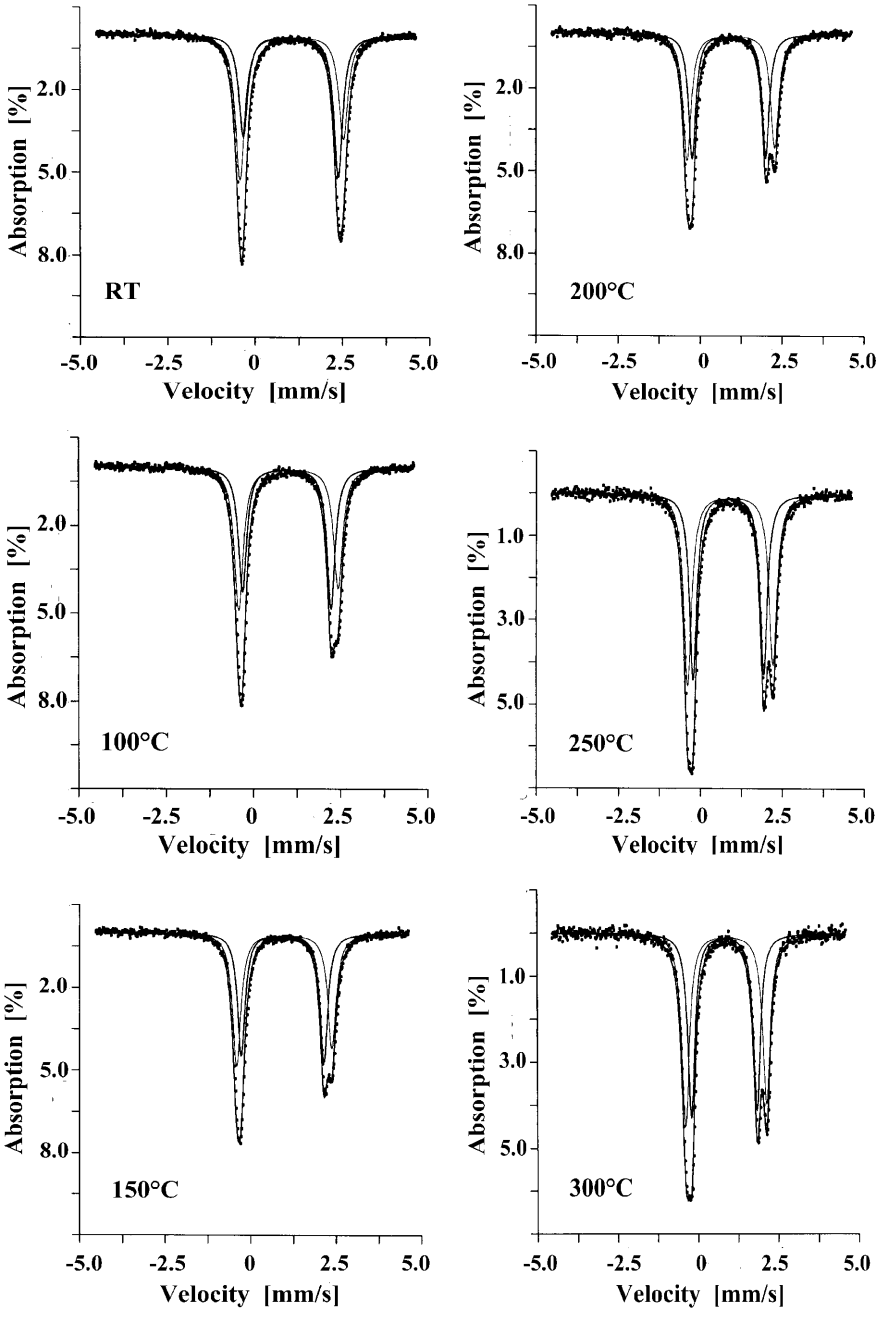

Fig. 1 Mössbauer spectra of a synthetic fayalite section with **k**//**a** at room temperature, 100, 150, 200, 250 and 300 K. The calculated total intensities and their two subspectra are represented by *solid lines*, the observed ones by *dots*

ligand contribution, as described above. The valence part is roughly proportional to the anisotropies

$$\Delta n_d = n_{x^2-y^2} + n_{xy} - n_{z^2} - (n_{xz} + n_{yz})/2$$
$$\Delta n_p = (n_x + n_y)/2 - n_z$$

of the Fe(3*d*)-shell and Fe(4*p*)-shell occupations, respectively. Usually the anisotropy of the Fe(3*d*)-shell dominates the efg for high-spin ferrous iron, whereas it is generally assumed that for high-spin ferric iron the ligand contribution should be the largest.

Model clusters

The construction of appropriate model clusters starts from the experimentally determined crystal structure (Table 3), and follows the experience from previous cluster calculations on minerals (Grodzicki and Amthauer 2000; Lougear et al. 2000; Grodzicki et al. 2001). These calculations have shown that reliable results for hyperfine parameters and magnetic properties are obtained only if large negative cluster charges are avoided and if at least the surroundings of each oxygen atom of the first coordination sphere of the central iron is being correctly described. Accordingly, model calculations on $[Fe(II)O_6]^{10-}$ clusters representing only the first coordination sphere are not suitable for studying the electronic properties of real minerals, but the cations of the second coordination sphere have to be included as well, comprising eight divalent iron and four (formally tetravalent) silicon atoms for $Fe^{M1}(II)$ and ten divalent iron and five silicon atoms for $Fe^{M2}(II)$. Each of these cations is sixfold (Fe)- or fourfold (Si)-coordinated by oxygen atoms leading to 34 and 38 oxygen atoms in the third shell of $Fe^{M1}(II)$ and $Fe^{M2}(II)$, respectively. Terminating the cluster at these oxygens gives, however, an inappropriate description of the electronic properties. First of all, the formal oxygen charge of −2 results in a large negative cluster charge that causes convergency problems if not compensated by a Madelung-type potential, e.g. of distributed point charges. Secondly, omitting the cations of the next shell bonded to the oxygens produces unsaturated O(2*p*) lone pairs that are in the same energy range as the Fe(3*d*) orbitals and may occasionally also cause convergency problems. Actually, both the bonding to the omitted cations and the Madelung potential will lead to a stabilization of these O(2*p*) orbitals, and thus would remove the convergency problems. This stabilization can be attained, of course, by adding further polyhedra, at the expense, however, of CPU time and memory space. Instead, experience has shown that generally the effect of these polyhedra can be simulated with sufficient accuracy either by replacing some or all oxygens of the third shell with fluorine atoms or by terminating them with one or two hydrogens in the direction of the next cations. Both together will reduce the cluster charge and will shift the 2*p*-orbitals into the energy range typical for the saturated O(2*p*)-orbitals. Such a procedure on one side keeps the size of the clusters manageable and, on the other side, provides a suitable model for the first coordination sphere of the central iron atom. Model calculations on clusters of various sizes show that size-converged results are obtained if all oxygen atoms beyond a distance of 4.20 Å from the central iron atom are replaced with fluorines and an appropriate number of hydrogens or polyhedra is added so that the neutrality of the total cluster is preserved. Finally, in order to avoid convergency problems, all Fe(II) ions of the second and higher coordination spheres can be substituted by magnesium atoms because the resulting changes in the computed spectroscopic data are within the error margins expected due to the general theoretical approximations. The resulting clusters with the composition $Fe^{M1}(II)O_6$–Si_4O_{10}–$Mg_8O_{18}F_6H_{10}$–$Si_8Mg_8F_{18}$ and $Fe^{M2}(II)O_6$–$Si_5O_4F_{10}$–$Mg_{10}O_3F_{21}$–Si_7F_{13} comprise 363 and 325 valence orbitals, respectively, and are thus large systems in a quantum chemical sense.

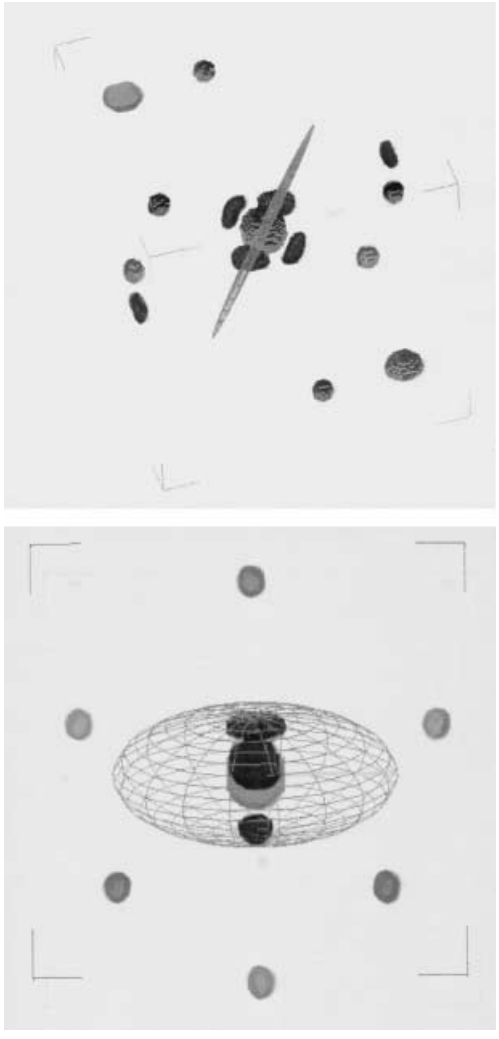

Fig. 2 Three-dimensional grey-scale plot of deformation electron densities around the Fe^{2+} positions in synthetic fayalite after the semiquantitative method. For better orientation, additional spherical densities around the iron and oxygen ions from Fourier inversion of F_{cal}. The electric field gradient tensor ellipsoid is displayed as a grid model. *Top* M1 position; *bottom* M2 site

Results

Optical spectra

A first criterion for the reliability of the calculations is provided by comparing the *d*-orbital energy differences with measured optical spectra of Fe-rich olivines (Burns 1993). The first coordination sphere of $Fe^{M1}(II)$ can roughly be characterized as a tetragonally elongated octahedron (approximate D_{4h} symmetry) with large axial Fe–O distances of 2.237 Å and almost identical Fe–O distances of 2.122 and 2.129 Å to the four equatorial oxygens. The first coordination sphere of $Fe^{M2}(II)$ may be considered as a trigonally distorted octahedron with three small Fe–O distances of 2.111 and 2.066 Å (2) to the upper triangle and with three large Fe–O distances of 2.236 and 2.296 Å (2) to the lower one.

The calculated energy level diagram is given in Fig. 4. The splitting of the e_g-like levels of $Fe^{M1}(II)$ is about 3000 cm^{-1} but merely 600 cm^{-1} for $Fe^{M2}(II)$. These

Table 3 Crystal data and structure refinement for sphere no.1 of synthetic fayalite, atomic coordinates and equivalent displacement parameters [with $U(\text{eq}) = 1/3Tr(U_{ij})^{\text{orth.}}$], anisotropic displacement parameters [with the exponential factor $-2\pi^2$ $(h^2a^{*2}U_{11}+\cdots+2h\,k\,a^*b^*U_{12})$]

Empirical formula	Fe_2SiO_4		
Formula weight	203.79		
Temperature	153 (2) K		
Wavelength	0.71073 Å		
Crystal system and space group	Orthorhombic, *Pnma*		
Unit-cell dimensions	a = 10.4597 (17) Å	b = 6.0818 (15) Å	c = 4.8150 (7) Å
	α = 90°	β = 90°	γ = 90°
Volume	306.30 (10) $Å^3$		
Form. units Z, calc. density	4	4.419 mg/m^3	
Absorption coefficient	9.690 mm^{-1}		
Theta range for data coll.	3.90 to 49.03°		
Limiting indices	$-21 \le h \le 20$	$-11 \le k \le 12$	$-9 \le l \le 9$
Reflections coll./unique	20712	1575	R (int) = 0.0273
Max. and min. transmission	0.196	0.137	
Refinement method	Full matrix least-squares on F^2		
Data/restraints/parameters	1575	0	41
Goodness-of-fit on F^2	1.156		
Final R indices ($I > 2\sigma(I)$)	$R1$ = 0.0223	$wR2$ = 0.0708	
R indices (all data)	$R1$ = 0.0249	$wR2$ = 0.0719	
Extinction coefficient	0.087 (4)		

Atomic coordinates ($\times 10^5$) and equivalent isotropic displacement parameters ($Å^2 \times 10^4$)

	x	y	z	U (eq)
Fe (1)	0	0	0	42 (1)
Fe (2)	28003 (2)	25000	98599 (4)	40 (1)
Si	9745 (3)	25000	43085 (8)	35 (1)
O (1)	9174 (9)	25000	76800 (20)	51 (1)
O (2)	−4688 (9)	25000	29110 (20)	49 (1)
O (3)	16580 (6)	3601 (11)	28842 (14)	53 (1)

Anisotropic displacement factors ($Å^2 \times 10^4$)

	U11	U22	U33	U23	U13	U12
Fe (1)	53 (1)	35 (1)	38 (1)	−3 (1)	1 (1)	−8 (1)
Fe (2)	39 (1)	32 (1)	50 (1)	0	0 (1)	0
Si	38 (1)	31 (1)	37 (1)	0	2 (1)	0
O (1)	60 (3)	50 (3)	42 (3)	0	3 (2)	0
O (2)	40 (3)	50 (3)	57 (3)	0	−1 (2)	0
O (3)	62 (2)	39 (2)	59 (2)	−4 (2)	2 (2)	10 (2)

values are in good agreement with the experimental data (Burns 1993), while the absolute values for Fe^{M1} (II) are somewhat larger than the measured ones. The splitting of the t_{2g} -like levels at the M1 site is about 20% smaller than at the M2 site but the splitting pattern is similar in both cases. This result demonstrates that considerable additional distortions superimpose the primary tetragonal and trigonal distortions of the Ml and M2 sites, respectively. Transitions between the t_{2g}-like levels have not yet been measured directly, but the temperature dependence of the efg provides an indirect, qualitative indication for the reliability of the calculated values (see below).

Electric field gradient

For high-spin ferrous iron in octahedral coordination the efg V_{zz} constitutes a sensitive criterion for the reliability of the calculated electronic structure since in this case the sign and size of the efg is related to the splitting pattern of the t_{2g}-like levels. The calculated quadrupole splittings given in Table 4 are +3.126 and +3.208 mm s^{-1} for the Ml and M2 sites, respectively, almost in quantitative agreement with the experimental values at low temperatures. Decomposition into the various contributions with respect to the principal axes system as described above demonstrates that in both cases the efg is dominated by the 3*d*-valence part related to the anisotropy of the Fe(3*d*) shell, whereas all the other contributions yield small corrections between 1 and 5% of the leading term.

The temperature dependence of the quadrupole splitting can be modelled by thermal occupation of the t_{2g}-like orbitals. Though only qualitative agreement can be expected in this case as, e.g. the influence of spin-orbit coupling and temperature-dependent geometry varia-

Table 4 Calculated quadrupole splitting (in mm/s), asymmetry parameter η and efg contributions for the M1 and M2 sites in fayalite

Site	ΔE_Q	η	val(3*d*)	val(4*p*)	coval.	ligand
M1	+3.126	0.72	+3.349	−0.034	−0.088	−0.101
M2	+3.208	0.36	+3.605	−0.113	−0.187	−0.097

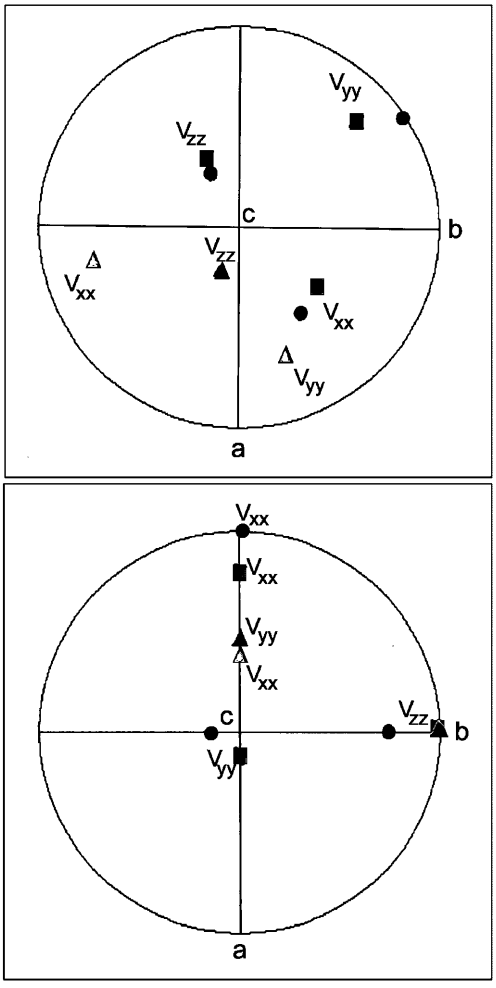

Fig. 3 Stereographic projection of the efg axes within the crystallographic axes system. efg evaluated experimentally (*circles*), semiquantitatively (*triangles*) and full-quantitatively (*squares*). *Closed* and *open symbols* refer to northern and southern hemisphere of the projection sphere, respectively. *Top* M1 position; *bottom* M2 site

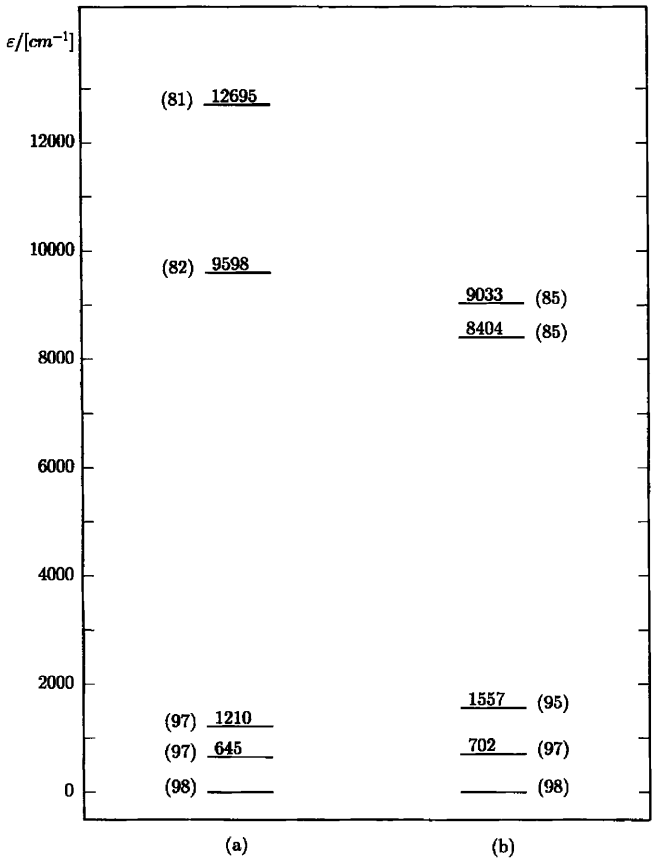

Fig. 4 Calculated energy level diagram according to the full-quantitative method. *Numbers in round brackets* give the percentage of 3*d* orbital admixture

tions are neglected, the calculated variation is almost in quantitative agreement with the experimental data (cf. Fig. 5).

The values of the quadrupole splitting determined semiquantitatively also match well with the theoretical slope at the temperature of the measured X-ray dataset.

The orientation of the three efg axes with respect to the crystallographic axis system was determined from the angles of Table 1 for the maximum temperatures, where the results are most reliable due to the enhanced splitting of the two doublets (Table 2, exp). This alignment is displayed together with the corresponding angles of the semi- and fully quantitative method (semi and full in Table 2, respectively). For the sake of clarity, the poles of the efg axes are plotted in a stereographic projection (Fig. 3).

There are two main comparisons to be drawn from the above datasets:

1. On M1, only the main component of the efg tensor is not too far away from the experimental one (semiquantitative method); on M2 the correspondence is better, with the exception that we observe in the Mössbauer refinement a symmetry break with respect to the mirror symmetry since two axes of the efg should lie in the mirror plane perpendicular to *b* (*Pnma*). These findings must be considered as reliable since the angle β ($=23°$) was directly adjusted and stable during all refinement procedures. The symmetry problem has been reported earlier and explained in terms of saturation effects of the peak intensities (Lottermoser et al. 1996).

2. For the M1 site, experimental and fully quantitative angles agree within 15°; the values for the M2 site exhibit again the discrepancy mentioned above as the fully quantitative procedure was performed under the requirements of *Pnma* symmetry.

Discussion

The observed discrepancy to symmetry requirements as detected by Mössbauer spectroscopy does not seem to be caused by a dominance of one subspectra over the other (as stated in our previous paper, Lottermoser et al. 1996) because the latter is the case only at comparably low temperatures; at room temperature or above, the two components of the fayalite pattern are equivalent. On the other hand, the non-vanishing β-angle value, not consistent with the mirror symmetry where β should be zero, has been detected at all measured temperatures with utmost reliability (minimum error) and seems to follow the trend already outlined in our previous paper (cf. Fig. 5b therein and Fig. 3, this publication). Hence, there is evidence for a slight symmetry break on M2 which, unfortunately, can be neither confirmed nor denied by our other investigations: the structure refinement was performed at low temperatures (152 K), where the effect is probably too small to be detected. The semi- and fully quantitative methods, on the other hand, rely on structural data with the symmetry requirements of *Pnma*, so that deviations from these cannot occur. Other structural investigations also do not yield any hint of a symmetry transformation at room temperature or above.

The other question, whether a semiquantitative refinement after our proceeding may lead to reliable efgs, can be confirmed at least in the case of fayalite – with some limitations.

The absolute values of the quadrupole splitting were well met, the direction of the main component V_{zz} agrees well with the expected orientation on M2 and not too badly on M1 (within 50°), taking the simplicity of the method into account. In addition, it should be noted that it was not possible to select the relevant difference density peaks with different render sizes "until the desired result comes up" because there was only a single combination of reasonable quadrupole splittings and efg angles at a definite render size which was identical for M1 and M2. At this point, there is still no onset of series termination errors, which we can identify without doubt, so that the contributions to the deformation densities are not influenced by artefacts. Consequently, the 3-D plots of Fig. 2 resemble to a high extent the quasi-3-D representation of the M1 and M2 polyhedra by Fujino et al. (1981), also in minor details (it should be noted that the latter authors used another space group!). For this reason, we are confident in the correctness of our starting point.

The minor components of the efg tensor, V_{xx} and V_{yy}, are only poorly matched by the semiquantitative method, especially on M1, most likely because we could only consider next-neighbour effects in our calculation. Whereas this is not essential for the M2 position, where the point symmetry is comparably high, for M1 a much larger cluster around the central Fe^{2+} should have been taken into account, as our fully quantitative approach has established. As the necessary memory size of the used computer system increases with the cube of the distance between the central ion and the surrounding deformation density peaks, we were not yet able to calculate with the necessary cell size because of machine limitations.

On the other hand, as our previous simulations show, the efg is directionally severely sensitive to the slightest changes in the surrounding charge densities, especially on low-dimensional sites – small shifts can cause a complete overturn of the relevant efg. Therefore, we may conclude that, with comparably large distances from the central ion, as used by our SCC-Xα calculations of the fully quantitative method, the results of the semiquantitative approach would have been better. In any case, the theoretical approach, with its rather high accordance between experiment and calculation, has taught us that large cluster sizes are essential for understanding the fayalite problem, while the restriction to nearest-neigh-

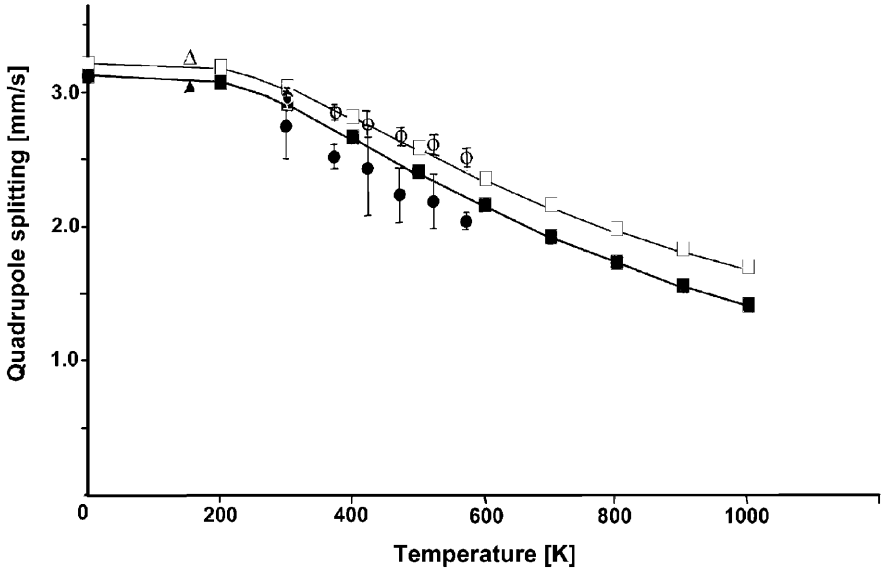

Fig. 5 Temperature dependence of quadrupole splitting determined experimentally (*circles*), semiquantitatively (*triangles*) and full-quantitatively (*squares*). The *closed* and *open symbols* refer to M1 and M2 position, respectively; the *solid lines* serve as eye guides

bour ions, as implied by the strong decrease of the potential, is insufficient.

Another supporting hint for the above interpretation is the magnetic behaviour of fayalite at low temperatures. The rather low-symmetrical M1 position displays a canted arrangement of magnetic Fe^{2+} moments coupled via superexchange to the collinearly ordered moments on the comparably high symmetrical M2 site. As the deformation electron density is strongly related to *d*-electron distributions, relevant for magnetism, it may be argued that the rather complicated magnetism on the M1 site is a measure for the stronger influence of neighbouring ions and the minor stability of the efg as compared to M2. Consequently, on M2, where the efg is rather stable, the magnetic moments keep their preferred orientation along *b* (in SG *Pnma*) at all temperatures below the Néel point.

Conclusions

The results of this study, combined with some unpublished earlier work, demonstrate that an estimate of the efg tensor with regard to the magnitude and direction of its main component is possible by evaluating 3-D deformation densities from X-ray diffractometry (semi-quantitative method). Minor details are obtainable only for comparably high-symmetrical sites, while for low-symmetrical positions the influence of asymmetrically surrounding charges leads to a severe instability of the efg with respect to its orientation. Spin-polarized SCC-Xα calculations (fully quantitative method) show that the efg becomes stable using large cluster sizes up to 97 atoms and that quantitative agreement between theory and experiment can be achieved. Hence, the results obtained with the semi-quantitative approach can only be understood on the basis of accurate theoretical evaluations. Though the described procedure holds true only for the synthetic fayalite in a strict sense, it may be generalized for other specimens. Other suitable samples are at present being considered for investigation.

Acknowledgements We wish to thank Dr. H. Kral for carefully grinding the fayalite microspheres used in X-ray diffractometry. Our study was supported by the Austrian Fonds zur Förderung der wisssenschaftlichen Forschung (FWF) under the contract number P11727-GEO. The electronic structure calculations were carried out at the Research Institute of Software Technology (RIST) in Salzburg.

References

Buerger MJ (1977) Kristallographie: eine Einführung in die geometrische und röntgenographische Kristallkunde. de Gruyter, Berlin

Burns RG (1993) Mineralogical applications of crystal field theory, 2nd ed. Cambridge University Press, pp 161–165

Eibschütz M, Ganiel U (1967) Sol St Comm 5: 267–270

Fuess H, Bats JW, Joswig W (1981) Elektronendichteverteilung in Fayalit α-Fe_2SiO_4 bei 120 K. Z Kristallogr 156: 41–43

Fujino K, Sasaki S, Takéuchi Y, Sadanaga R (1981) X-ray determination of electron distributions in forsterite, fayalite and tephroite. Acta Crystallogr (B)37: 513–518

Gonser K (1975) From a strange effect to Mössbauer spectroscopy. In: Gonser K (ed) Topics in applied physics, vol 5. Mössbauer spectroscopy. Springer, Berlin Heidelberg New York, pp 1–51

Grodzicki M (1980) A self-consistent-charge Xα method. J Phys (B)13: 2683–2692

Grodzicki M (1985) Theorie und Anwendungen der Se1f-Consistent-Charge-Xα Methode. Thesis of habilitation, Hamburg 1985

Grodzicki M, Amthauer G (2000) Electronic and magnetic structure of vivianite: cluster molecular orbital calculations. Phys Chem Miner 27: 694–702

Grodzicki M, Männing V, Trautwein AX, Friedt JM (1987) Calibration of isomer shifts and quadrupole coupling constants for ^{119}Sn, ^{127}I and ^{129}I as derived from SCC-Xα calculations and Mössbauer measurements. J Phys (B)20: 5595–5625

Grodzicki M, Heuss-Assbich1er S, Amthauer G (2001) Mössbauer investigations and molecular orbital calculations on epidote, Phys Chem Miner (in press)

IDL® Interactive Data Language Vers. 5.3, Research Systems Corp., 4990 Pearl East Circle, Boulder CO 80301 (www.rsinc.com)

Lauer S, Marathe VR, Trautwein AX (1979) Sternheimer shielding using various approximations. Phys Rev (A)19: 1852–1861

Lottermoser W, Forcher K, Kaliba P (1988) MOESALZ: an interactive Mössbauer spectra refinement program. University of Salzburg

Lottermoser W, Forcher K, Amthauer G, Fuess H (1995) Powder- and single-crystal Mössbauer spectroscopy on synthetic fayalite. Phys Chem Miner 22(4): 259–267

Lottermoser W, Forcher K, Amthauer G, Treutmann W, Hosoya S (1996) Single-crystal Mössbauer spectroscopy on the three principal sections of a synthetic fayalite sample in the antiferromagnetic state. Phys Chem Miner 23(7): 432–438

Lottermoser W, Schell T, Steiner K (1999) A time-minimizing hybrid method for fitting complex Mössbauer spectra. Program and Abstracts ICAME 99, Garmisch-Partenkirchen: T9/33

Lougear A, Grodzicki M, Bertoldi C, Trautwein AX, Steiner K, Amthauer G (2000) Mössbauer and molecular orbital study of chlorites. Phys Chem Miner 27: 258–269

Rager H, Schmidt PC (1981) Electric field calculation in forsterite Mg_2SiO_4. Phys Chem Miner 7: 169–176

Ray SN, Das TP (1977) Nuclear quadrupole interaction in the Fe^{2+} ion inducing many-body effects. Phys Rev (B)16: 4794–4804

Sheldrick G (1997) SHELX-97, program for the solution and refinement of crystal structures. University of Göttingen, Germany

Sheldrick G (2000) SADABS, program for empirical absorption correction for area detector data. University of Göttingen, Germany

Slater JC (1974) Quantum theory of molecules and solids vol. 4. McGraw-Hill, New York

Steiner K, Lottermoser W, Leeb H, Amthauer G (1998) Neue Darstellungs- und Analysemöglichkeiten von 3-D Elektronendichten, 6. Jahrestagung der DGK, Karlsruhe, Referate: 200

Steiner K, Schell T, Lottermoser W (1999) A time-minimizing hybrid method for fitting complex Mössbauer spectra. Phys Chem Miner 27: 34–40

Thong N, Schwarzenbach D (1979) The use of electric field gradient calculations in charge density refinements. II. Charge density refinement of the low-quartz structure of aluminum phosphate. Acta Crystallogr (A)35: 658–664